Supplemental Information

Activated gp130 signaling selectively targets B cell differentiation to induce mature lymphoma and plasmacytoma

Running titel: Gp130 activation causes lymphoma and plasmacytoma

Anna K. Scherger[1], Mona Al-Maarri[2], Hans C. Maurer[3], Markus Schick[1], Sabine Maurer[1], Rupert Öllinger[3-5], Irene Gonzalez-Menendez[6], Manuela Martella[6], Markus Thaler[7], Konstanze Pechloff[4,7,8], Katja Steiger[8,9], Sandrine Sander[10], Jürgen Ruland[4,7,8], Roland Rad[3-5,8], Leticia Quintanilla-Martinez[6], Frank T. Wunderlich[2], Stefan Rose-John[11], and Ulrich Keller[1,8,12]

[1] Internal Medicine III, Technische Universität München, Munich, Germany
[2] Max Planck Institute for Metabolism Research, Center for endocrinology, preventive medicine and diabetes, Cologne, Germany
[3] Internal Medicine II, Technische Universität München, Munich, Germany
[4] Center for Translational Cancer Research (TranslaTUM), Technische Universität München, Munich, Germany
[5] Institute of Molecular Oncology and Functional Genomics, Technische Universität München, Munich, Germany
[6] Institute of Pathology, Eberhard-Karls-Universität Tübingen, Tübingen, Germany
[7] Institute of Clinical Chemistry and Pathobiochemistry, Technische Universität München, Munich, Germany
[8] German Cancer Consortium (DKTK) and German Cancer Research Center (DKFZ), Heidelberg, Germany
[9] Institute of Pathology, Technische Universität München, Munich, Germany
[10] Adaptive Immunity and Lymphoma, German Cancer Research Center/ National Center for Tumor Diseases Heidelberg (NCT), Heidelberg, Germany
[11] Institute of Biochemistry, Christian-Albrechts-Universität zu Kiel, Kiel, Germany
[12] Department of Hematology and Oncology, Charité - Universitätsmedizin Berlin, Campus Benjamin Franklin, Berlin, Germany

A.K.S. and M.A.M. contributed equally to this study.

Contact information for correspondence:
Ulrich Keller, Department of Hematology and Oncology, Charité - Universitätsmedizin Berlin, Campus Benjamin Franklin, Berlin, Germany, phone -49-30-450-513381; fax -49-89-41404879; E-mail: ulrich.keller@charite.de

Supplemental Materials and Methods

Plasmids

L-gp130, the constitutively active form of gp130, was described previously (1). MSCV-L-gp130-IRES-GFP was cloned by digesting the MSCV-IRES-GFP plasmid with EcoRI and BglII (Fermentas) following a PCR for L-gp130 with primers containing overhangs for EcoRI and NcoI restriction (Omniscript RT Kit; Qiagen). Ligation was performed using the Quick T4 DNA Ligase (New England Biolabs). MSCV-CRE-IRES-YFP was a gift from Marc Schmidt-Supprian.

Generation of retrovirus and transfection of MEFs

Retrovirus was obtained through transient infection of Phoenix E cells with Lipofectamine 2000 (Invitrogen) according to the manufacturer's instructions. MEFs were infected three times at 12-hour intervals with retrovirus supplemented with 8 µg/ml polybrene (Sigma-Aldrich). MEFs were then sorted for GFP/YFP positivity on the BD FACSAria™ III cell sorter (BD Biosciences) for further analyses.

Real-time PCR and gene expression analysis

Complementary DNA (cDNA) from MEFs was reverse transcribed using the Omniscript® RT Kit on mRNA isolated with the RNeasy® Mini Kit (both from Qiagen) according to the manufacturer's protocols. Real-time PCR was performed using Platinum SYBR-Green Q PCR SuperMix-UDG (Invitrogen) on ABI Prism 7700 (Applied Biosystems). Data analysis was done by comparing Ct values with a control sample set as 1 and normalized to the expression of GAPDH. Sequences for primers are given in supplemental Table S1.

Immunoblotting

Cell lysis for immunoblotting was performed with lysis buffer containing 50 mM HEPES (pH 7.5), 150 mM NaCl, 1 mM EDTA, 2.5 mM EGTA, 0.1 % Tween-20 (all from Sigma-Aldrich), and protease inhibitors (Roche) followed by sonication (4 cycles with 10 sec at 30 % power). Protein extracts (15 µg per lane) were electrophoretically separated on a 10 % SDS-PAGE gel, transferred to PVDF-membranes (Millipore) and probed with antibody. The following antibodies were used: anti-gp130 (sc-655, Santa Cruz Biotechnology

Inc.), anti-STAT3 (#4904), anti–P-STAT3 (#9145) (all Cell Signaling Technology), and anti–β-Actin (A5441, Sigma-Aldrich).

Generation of *R26 fl rx L-gp130* mice

To generate the parental *R26 fl rx L-gp130* strain, we have employed the novel B9-36 ROSA26 targeting vector, a derivative of the STOP-EGFP ROSA CAG targeting vector, comprising a short arm of homology (SAH), a chicken beta actin promoter followed by a loxP flanked neo stop and a rox flanked stop cassette. The single AscI site can be used to insert in frame transgenes to the 2A driven ZsGreen construct to monitor Cre- and Dre-mediated recombination. 3' to the 2A ZsGreen cassette, the 4.5 kb long arm of homology (LAH) and negative PGK DTA cassettes are inserted. L-gp130 was amplified from pCDNA L-gp130 with oligos 5AscLGP130 (GGC GCG CCA CCA TGT TGA CGT TGG CAG ACT TGG) and 3AscLGP130 (GGC GCG CCC TGA CCT GAG GCA TGT AGC CGC C) sequenced and inserted into AscI site of B9-36 TV. 40 µg of AsiSI linearized B9-36 L-gp130 was transfected into 10^7 Bruce 4 ES cells by electroporation and selected with G418. Isolated single ES clones were screened using Southern blot analysis of EcoRI digested clonal DNA using ROSA26 EcoRI/PacI probe as previously described (2). An additional 7.1 kb targeted band appeared with the 15.6 kb WT band in correctly targeted clones. A neo probe confirmed single integration of the transgene. Correctly targeted clones were injected into donor blastocysts to generate chimeric mice that were backcrossed to C57BL/6 mice to obtain *R26 fl rx L-gp130* mice on a pure C57BL/6 background. To create the Cre-activatable *L-gp130* conditional allele, parental mice were crossed to Dre deleter mice (3).

HSPC-FLC transplantation

HSPC-FLCs were obtained on day 13.5 after mating. C57BL/6 HSPC-FLC recipient mice received myeloablative irradiation (8.5 Gy) and were transplanted with 1.2 x 10^6 syngeneic FLC together with 0.2 x 10^6 Ly5.1 BM support in total via tail vein injection. Recipient C57BL/6 mice for transplantation experiments were purchased from Charles River Laboratories or Janvier Laboratories and were, as all other mice in this study, monitored for signs of morbidity and tumor development by daily observation and physical examination. Tumors were harvested after mouse sacrifice, and cells were frozen viable.

Serial transplantation of tumor cells

For serial transplantation, sick *CD19;L-gp* mice were sacrificed and 1 x 10^6 tumor cells were transplanted into sublethally irradiated (4.5 Gy) syngeneic recipients. Recipient C57BL/6 mice for transplantation experiments were purchased from Charles River Laboratories or Janvier Laboratories and were monitored for signs of morbidity and tumor development by daily observation and physical examination. Tumors were harvested after mouse sacrifice, and cells were frozen viable.

Tissue and organ samples

Blood samples were collected into 1.2 ml heparinized tubes (Sarstedt). Blood cells were counted on a Scil Vet ABC (ScilAnimal Care). BM cells were flushed from femurs and tibias with $HF2^+$ buffer (Hank's balanced salt solution, supplemented with 2 % FCS, 10 mM HEPES buffer and antibiotics, Thermo Fisher Scientific). Spleens and tumors were passed through 100 µm nylon Cell Strainers (BD Biosciences). Viable cells were counted using Trypan Blue (Invitrogen).

Serum electrophoresis

Serum protein electrophoresis was performed on an Elphoscan ES2000 Plus device (Sarstedt). Briefly, 25 µl mouse serum was applied to a cellulose acetate strip. After separation, the resulting protein fractions were stained with Ponceau S (Sarstedt) and quantified by densitometric scanning.

Analysis of IgH rearrangements

IgH rearrangements were amplified by PCR from genomic DNA as follows: MsVHe-AH-forward (TCGAGTTTTTCAGCAAGATGAGGTGCAGCTGCAGGAGTCTGG) was combined with JH4e-New-AH-reverse (ATCTTCTAGAAAGATGTCCCTATCCCATCATCCAGGG) to amplify rearrangements involving JH1-4. All samples were amplified by PCR for 35 cycles with Phusion High Fidelity DNA Polymerase (2 U/µl) (Thermo Fisher Scientific) with the following conditions: 2 mM $MgCl_2$; melt at 98 °C for 10′00″, anneal at 72 °C for 1′00″, extend at 72 °C for 10′00″ and then visualized on a 1 % agarose-gel. Genomic DNA from *Eµ-Myc* LNs was used for monoclonal and oligoclonal controls.

Magnetic cell separation

Murine B cells and plasma cells were magnetically purified from tumor material as well as from young *CD19;L-gp* and C57BL/6 WT control spleens using CD19 and/or CD138 micro beads according to the manufacturer's protocol (130-052-201 and 130-092-530, Miltenyi Biotec). Purification was afterwards controlled by flow cytometry.

RNA-sequencing

Library preparation for bulk 3'-sequencing of poly(A)-RNA was done as described previously (4). Briefly, barcoded cDNA of each sample was generated with a Maxima RT polymerase (Thermo Fisher Scientific) using oligo-dT primer containing barcodes, unique molecular identifiers (UMIs) and an adapter. 5' ends of the cDNAs were extended by a template switch oligo (TSO) and after pooling of all samples full-length cDNA was amplified with primers binding to the TSO-site and the adapter. cDNA was tagmented with the Nextera XT kit (Illumina, San Diego, CA, USA) and 3'-end-fragments finally amplified using primers with Illumina P5 and P7 overhangs. In comparison to Parekh et al. the P5 and P7 sites were exchanged to allow sequencing of the cDNA in read1 and barcodes and UMIs in read2 to achieve a better cluster recognition. The library was sequenced on a NextSeq 500 (Illumina) with 75 cycles for the cDNA in read1 and 16 cycles for the barcodes and UMIs in read2.

Data was processed using the published Drop-seq pipeline (v1.0) to generate sample- and gene-wise UMI tables (5). Reference genome (GRCm38) was used for alignment. Transcript and gene definitions were used according to the ENSEMBL annotation release 75.

Statistical analysis of high-throughput gene expression data

High-throughput gene expression data from the conditions indicated in the text were carried out using the R environment for statistical computing (v3.4.0) (6).

Data acquisition and pre-processing

B cell development: gene expression data from studies comparing different stages of B cell development using the Affymetrix GeneChip Human Genome U133 Plus 2.0 platform were retrieved from ArrayExpress

and Gene Expression Omnibus (GEO), respectively. Specifically, the accession numbers were E-MEXP-2360 (7), E-MEXP-3034 (8), E-MEXP-3945 (9), and GSE15271 (10).

CEL files were retrieved for all studies and normalized using the *GCRMA* R package (11).

Multiple myeloma: Normalized gene expression data from Keats et al. (12) were retrieved from the Multiple Myeloma Genomics Portal (13).

For all microarray datasets, probes were collapsed at the gene level by keeping the probe with the highest median expression. Genes with an interquartile range of zero were removed from the analysis.

Differential gene expression analysis

Genome-wide differential gene expression analysis for RNA-Seq data was carried out using the *voom-limma* framework as implemented the R package *limma* (14). This yielded moderated t- and F-statistics for two and three group comparisons, respectively, and a false discovery rate (FDR) < 0.1 was considered significant.

Gene set collection

Gene sets were retrieved from the MSigDb v6.0 (15,16) modules HALLMARK, C2 canonical pathways, C3 transcription factor targets and C6 oncogenic signatures and were categorized as follows: (i) B cell signaling pathways whose names contain ‘B_CELL’ or ‘BCR’ (n = 10), (ii) NF kappa B signaling pathways containing ‘KAPPAB', or ‘NFKB’ (n = 22), (iii) Downstream signaling pathways containing ‘MAPK’, ‘ERK’, ‘PI3K’, ‘AKT’ or ‘MTOR’ (n = 43), (iv) Hippo signaling containing ‘HIPPO’ or ‘YAP’ (n = 5), (v) Developmental pathways containing ‘WNT’, ‘NOTCH’, ‘TGF’, ‘HEDGEHOG’, ‘SHH’ or ‘BMP’ (n = 40) and (vi) MYC and STAT3 signaling containing ‘MYC’, ‘IL6’, ‘IL6ST’ or ‘STAT3’ (n = 18). In order to determine STAT3 activity as opposed to mere STAT3 expression among different B cell development stages, the expression of STAT3 target genes rather than STAT3 itself was considered as described below. STAT3 target genes were retrieved from the TTRUST (17) database.

Single sample gene set enrichment

We used single sample GSEA (ssGSEA) to determine the activity of select pathways or regulatory genes per individual sample as implemented in the VIPER (virtual inference of protein activity by enriched regulon

analysis) framework (18). VIPER is capable to account for separate tails of a gene set, e.g. up- and downregulated genes from a signature between conditions, and furthermore, considers the absolute ranking of genes as well by using the aREA algorithm (19).

First, raw counts from RNA sequencing were normalized to account for different library sizes, and the variance was stabilized by transforming the data to $\log_2$ CPM (counts per million) using the *edgeR* (20) R package. Then ssGSEA was carried out using the indicated gene sets and regulons, respectively, and the *viper(eset.filter = FALSE, method = 'scale', min.size = 10)* function from the eponymous R package (18). VIPER yields normalized enrichment scores (NES) per sample which are normally distributed and based on the assumption that in the null situation, the target genes are uniformly distributed in the gene expression signature.

Differential enrichment analysis of gene sets and regulatory gene activity between conditions was carried out using the *limma* R package (14) and a false discovery rate (FDR) < 0.1 was considered significant. If only one pathway or signature was compared across conditions, significance was assessed using Welch's t-test and ANOVA assuming unequal variance as implemented in the R *stats* package, respectively, depending on whether two or more conditions were being compared. Single sample enrichment results for select pathways were depicted in a heatmap using the pheatmap R package (21).

Derivation of a *CD19;L-gp* gene expression signature

First we carried out differential gene expression analysis between wild type B cells and B cells with Cre-mediated L-gp130 activation (*CD19;L-gp*) as described above yielding a total of 2094 genes which were differentially expressed at a FDR < 0.05. The top 100 genes induced and repressed by L-gp130 activation, respectively, were used to build a two-tailed gene set and information on their effect size ($\log_2$ fold change) was added as an additional weight for ssGSEA, thus yielding a *L-gp130 signature regulon*. When using the L-gp130 signature regulon, positive enrichment scores indicate similarity to *CD19;L-gp* B cells whereas negative enrichment scores indicate similarity to wild type B cells.

Differential expression of immunoglobulin heavy and light chain genes

Immunoglobulin (Ig) light (*Igkc, Iglc1, Iglc2, Iglc3, Iglc4*) and heavy (*Igha, Ighm, Ighd, Ighg2b, Ighg3, Ighg1, Ighg2c*) chain genes were examined for their differential expression between WT and tumor tissues from

Vav;L-gp mice, *CD19;L-gp* mice with PC and Mature phenotypes, respectively. Expression levels are shown as counts per million (CPM) on a log2 scale and false discovery rates were retrieved from a linear model fit using the R package *limma* (14).

ELISA

Basal Ig concentrations of IgM and IgG_{total} were determined by ELISA applying the SBA Clonotyping™ System-AP (SouthernBiotech) and the Mouse Immunoglobulin Panel (SouthernBiotech). Optical densities were measured on a Sunrise Microplate Reader (Tecan) with Magellan 7 software. Statistical analysis was performed via Student's *t* test or ANOVA test followed by the Tukey test on GraphPad Prism7 (GraphPad Inc.).

Flow cytometry

Fluorescently labeled antibodies (all from BD Pharmingen, eBioscience or BioLegend) were used against the following murine surface proteins: CD45 (clone 30-F11), CD3e (clone 145-2C11) B220 (clone RA3-6B2), CD11b (clone M1/70), Gr.1 (clone RB6-8C5), CD19 (clone 1D3), CD95 (clone Jo2), GL7 (clone GL7), CD138 (clone 281-2), IgM (clone II/41), and IgD (clone 11-26). For hematopoietic precursor compartments the Mouse Hematopoietic Lineage Biotin Cocktail was used together with Streptavidin, c-kit (clone 2B8), Sca-1 (clone D7), and Ter119 (clone Ter-119) (all from eBioscience) for defining LSK and MPP compartments in the BM. Gating for these populations has been described elsewhere (22). Data were acquired on a Cyan ADP Lx P8 (Coulter-Cytomation). FlowJo Software (Tree Star Inc.) was used for data analysis.

Immunohistochemistry

Immunohistochemistry was performed with antibodies directed against B220/CD45R (#550286, BD Pharmingen, dilution 1:50), CD138 (#553712, BD Pharmingen, 1:1000), CD3 (#C1597C01, DCS, 1:50), Myeloperoxidase (MPO) (#RB-373-R7, NeoMarkers, rtu), Ki67 (#Kl681R06, DCS, rtu), Myc (#ab32072, Abcam, 1:200), IgM (#A0425, Dako, 1:10000), and Pax5 (#610863, BD Pharmingen, 1:10).

Supplemental References

1. Stuhlmann-Laeisz C, et al. Forced dimerization of gp130 leads to constitutive STAT3 activation, cytokine-independent growth, and blockade of differentiation of embryonic stem cells. *Mol Biol Cell.* 2006;17(7):2986-2995.
2. Belgardt BF, et al. PDK1 deficiency in POMC-expressing cells reveals FOXO1-dependent and -independent pathways in control of energy homeostasis and stress response. *Cell Metab.* 2008;7(4):291-301.
3. Anastassiadis K, et al. Dre recombinase, like Cre, is a highly efficient site-specific recombinase in E. coli, mammalian cells and mice. *Dis Model Mech.* 2009;2(9-10):508-515.
4. Parekh S, Ziegenhain C, Vieth B, Enard W, Hellmann I. The impact of amplification on differential expression analyses by RNA-seq. *Sci Rep.* 2016;6:25533.
5. Macosko EZ, et al. Highly Parallel Genome-wide Expression Profiling of Individual Cells Using Nanoliter Droplets. *Cell.* 2015;161(5):1202-1214.
6. R-Core-Team. R: A Language and Environment for Statistical Computing. In. R Foundation for Statistical Computing, Vienna, Austria2016.
7. Jourdan M, et al. An in vitro model of differentiation of memory B cells into plasmablasts and plasma cells including detailed phenotypic and molecular characterization. *Blood.* 2009;114(25):5173-5181.
8. Jourdan M, et al. Characterization of a transitional preplasmablast population in the process of human B cell to plasma cell differentiation. *J Immunol.* 2011;187(8):3931-3941.
9. Jourdan M, et al. IL-6 supports the generation of human long-lived plasma cells in combination with either APRIL or stromal cell-soluble factors. *Leukemia.* 2014;28(8):1647-1656.
10. Caron G, Le Gallou S, Lamy T, Tarte K, Fest T. CXCR4 expression functionally discriminates centroblasts versus centrocytes within human germinal center B cells. *J Immunol.* 2009;182(12):7595-7602.
11. Wu J, R. Irizarry, J. MacDonald, J. Gentry. gcrma: Background adjustment using sequence information. In. Vol R package version 2.38.0.2014.
12. Keats JJ, et al. Promiscuous mutations activate the noncanonical NF-kappaB pathway in multiple myeloma. *Cancer Cell.* 2007;12(2):131-144.

13. Liefeld T, Q. Gao, M. A. Chapman, G. Tonon, D. Auclair, M. Reich, and T. R. Golub. The Multiple Myeloma Genomics Portal. *Blood.* 2008;112(11):5115-5115.

14. Ritchie ME, et al. limma powers differential expression analyses for RNA-sequencing and microarray studies. *Nucleic Acids Res.* 2015;43(7):e47.

15. Subramanian A, et al. Gene set enrichment analysis: a knowledge-based approach for interpreting genome-wide expression profiles. *Proc Natl Acad Sci U S A.* 2005;102(43):15545-15550.

16. Liberzon A, Birger C, Thorvaldsdottir H, Ghandi M, Mesirov JP, Tamayo P. The Molecular Signatures Database (MSigDB) hallmark gene set collection. *Cell Syst.* 2015;1(6):417-425.

17. Han H, et al. TRRUST v2: an expanded reference database of human and mouse transcriptional regulatory interactions. *Nucleic Acids Res.* 2018;46(D1):D380-D386.

18. Alvarez MJ, F. Giorgi, and A. Califano. Using viper, a package for Virtual Inference of Protein-activity by Enriched Regulon analysis. *Bioconductor.* 2014:1-14.

19. Alvarez MJ, et al. Functional characterization of somatic mutations in cancer using network-based inference of protein activity. *Nat Genet.* 2016;48(8):838-847.

20. Robinson MD, McCarthy DJ, Smyth GK. edgeR: a Bioconductor package for differential expression analysis of digital gene expression data. *Bioinformatics.* 2010;26(1):139-140.

21. Kolde R. *pheatmap: Pretty Heatmaps.* https://CRAN.R-project.org/package=pheatmap: *R package version*;2015.

22. Istvanffy R, et al. Stromal pleiotrophin regulates repopulation behavior of hematopoietic stem cells. *Blood.* 2011;118(10):2712-2722.

Supplemental Figure Legends

Supplemental Figure S1. Expression and activity of STAT3 - hierarchical cluster analysis

A. Immunoblot analysis of $CD19^+$ B cells from six weeks old *CD19;L-gp* mice as well as *L-gp* and *CD19Cre* controls using the indicated antibodies. L-gp130 was detected using a gp130 antibody. L-gp130 expression indicates efficient Cre-mediated recombination. The data shown are from one representative experiment with n = 3 animals per group.
B. Spleens from *CD19;L-gp* and age-matched *L-gp* controls do not show significant differences in weight (n = 3). Shown are means ± SEM.
C. Histological analysis (H&E staining) of spleen and BM from a representative young *CD19;L-gp* mouse in comparison to an age-matched *L-gp* control. Original magnification, x400. H&E: Hematoxylin&Eosin.
D. Analysis of PB from young mice and age-matched controls does not reveal significant differences in in WBC, or in lymphocyte (Lymph), and granulocyte (Gran) frequencies (n = 3). Shown are means ± SEM.
E. Flow cytometric analysis of BM, spleen, and PB show no significant differences between T cell (left) and B cell (right) compartments in compound mice as compared to *L-gp* controls (n = 3). Shown are means ± SEM.
F. The top 100 up- and downregulated genes from (B) were chosen from the 2094 DEG based on their effect size (log_2 fold change) and represent the L-gp130 signature for further analysis. GSEA on the original signature illustrates their enrichment on their respective end of the signature.
G. ssGSEA results of the L-gp130 signature among various stages of B cell development with highest enrichment results in activated B cells and GC B cells.

Supplemental Figure S2. Flow cytometry gating strategy

Shown is the flow cytometry gating strategy used throughout the study to determine distinct subsets and the state of B cell differentiation. First, doublets were excluded, followed by exclusion of debris and red blood cells (RBC) via cell size and granularity (FSC/SSC). Propidium iodide (PI) was then used to eliminate dead cells. Pro-/pre and immature B cells were defined by gating for B220 vs. IgM. Plasma cells were

defined as $CD138^{+}CD19^{-}$ while further gating on the $CD19^{+}$ B cell population defined GC B cells via GL7 staining. Surface expression of immunoglobulins IgM and IgD revealed the maturity state of B cells. The previous gate is always indicated as is the organ analyzed.

Supplemental Figure S3. Gp130 activation in B cell by means of CD19Cre results in a transplantable B cell malignancy

A. Histological analysis (H&E staining) showing infiltration of tumor cells into the BM, spleen, and mesenteric nodal tumor of a representative diseased *CD19;L-gp* mouse of the PC phenotype (upper panel) as well as the Mature phenotype (lower panel) as defined by flow cytometric analysis. At least 10 mice per genotype were analyzed. Original magnification, x400. H&E: Hematoxylin&Eosin.
B. Extent of infiltration of tumor cells of the PC phenotype (left, n = 23) and Mature phenotype (right, n = 23) into BM, spleen, and mesenteric nodal tumor of diseased mice as assessed by flow cytometry.
C. Flow cytometric analysis of one representative diseased *CD19;L-gp* mouse allocated to the PC phenotype revealing infiltration of distinct B cell populations into the different organs.
D. Ig levels, assessed by ELISA, from serum of sick *CD19;L-gp* mice of the Mature (n = 6) and PC (n = 4) phenotype in comparison to *CD19* (n = 5) and *L-gp* (n = 4) controls. Differences in IgM (left) and IgG levels (right) were considered not significant as determined by the ANOVA test. Shown are means ± SEM.
E. RNA-Seq gene expression profiles of Ig heavy chain constant regions obtained from mesenteric nodal tumor material of *CD19;L-gp* of the Mature and PC phenotypes in comparison to $CD19^{+}$ isolated WT splenocytes. CPM: counts per million, FDR: false discovery rate. Significance was evaluated by the ANOVA test with subsequent assessment of the FDR.
F. RNA-Seq gene expression profiles of Ig light chain constant regions obtained from mesenteric nodal tumor material of *CD19;L-gp* of the Mature and PC phenotypes in comparison to $CD19^{+}$ isolated WT splenocytes. CPM: counts per million, FDR: false discovery rate. Significance was evaluated by the ANOVA test with subsequent assessment of the FDR.
G. Kaplan-Meier curve showing survival of serially transplanted *CD19;L-gp* mice. 1×10^{6} tumor cells were transplanted into sublethally (4.5 Gy) irradiated syngeneic recipients via tail vein injection.

Graft recipients showed a median survival of 116 days. Results are representative for five independent experiments with n = 3 recipients per primary tumor.

H. Flow cytometric analysis of a representative sick donor and recipient *CD19;L-gp* mouse displaying serial transplantability of the $CD138^+$ disease.

Supplemental Figure S4. Activation of gp130 in GC B cells, phenotype

A. Histological analysis (H&E staining) showing infiltration of tumor cells into the BM, spleen, and mesenteric nodal tumor of a representative diseased *Cg1;L-gp* mouse (upper panel) as well as a representative diseased *Blimp1;L-gp* mouse (lower panel). At least 3 mice per genotype were analyzed. Original magnification, x400. H&E: Hematoxylin&Eosin.

B. Flow cytometric analysis of a representative diseased *Blimp1;L-gp* mouse with a PC phenotype showing infiltration of malignant $CD138^+$ plasma cells into all organs assessed.

C. Upper panel: Serum protein electrophoresis from representative diseased *Cg1;L-gp* mice. Lower panel: Serum protein electrophoresis from representative *Blimp1;L-gp* mice. The bars indicate the percentage of mice with (w/) or without (w/o) gammopathy. At least 8 mice per genotype were analyzed.

D. Ig levels, assessed by ELISA, from serum of diseased *Cg1;L-gp* mice (n = 9) in comparison to *L-gp* controls (n = 4). The outlier presenting with low IgG level did also not show evidence of monoclonal gammopathy as assessed by serum protein electrophoresis. Shown are means ± SEM. (** P = 0.0051, by the student's *t* test).

Supplemental Figure S5. The L-gp130 signature is represented during progression of human MM

ssGSEA results of the L-gp130 signature as identified and defined in Supplementary Figure S2 among different progression stages of MM. These stages were previously profiled by Keats et al. Enrichment results are positively correlated with disease progression.

Supplemental Figure S6. Activated gp130 collaborates with B cell-targeted Myc, phenotype

Flow cytometric analysis of spleen and BM from all three indicated genotypes displaying the same phenotype as seen in the respective nodal tumors. At least 3 mice per genotype were analyzed. Shown are representative analyses.

Supplemental Figure S7. Activation of gp130 in HSPCs by means of VavCre, phenotype

A. Flow cytometric analysis revealing genetic activation of L-gp130 expression in nearly all $PI^{-}CD45^{+}$ cells from diseased *Vav1;L-gp* as defined by ZsGreen positivity. In contrast, *Vav1* and *L-gp* controls cells did not show a ZsGreen signal. Depicted is the BM of one representative animal per cohort. At least 4 mice per cohort were analyzed.
B. Splenocytes from diseased *Vav1;L-gp* show strong activation of gp130 signaling as assessed by pSTAT3 expression, immunoblot analysis. *Vav1;L-gp* mice express the L-gp130 protein.
C. Flow cytometric analysis of BM from diseased *Vav1;L-gp* animals displaying no significant differences in the $Lin^{-}Sca1^{+}c\text{-}kit^{+}$ (LSK) as well as $Lin^{-}Sca1^{-}c\text{-}kit^{+}$ (MPP) compartments in comparison to age-matched control groups. ANOVA testing was performed. Shown are means ± SEM of at least 4 mice per group.
D. T cells are the major leucocyte subpopulation of living $ZsGreen^{+}$ cells in LNs from diseased *Vav1;L-gp* as determined by flow cytometry (n = 11). Shown are means ± SEM.
E. Immunohistochemical analysis from spleen (left) and LN (right) of a representative diseased *Vav1;L-gp* showing infiltration of $CD3^{+}$ T cells into the LN. Pax5 staining is seen in both organs, as is IgM expression. Ki67 staining reveals a higher proliferation rate in the spleen as compared to the LN. Original magnification, x400.
F. Serum protein electrophoresis from one representative *Vav1;L-gp* animal indicative of moderate but significant monoclonal gammopathy. The arrow indicates the abnormal protein fraction. All tested animals presented with this feature (n = 15).
G. Ig levels, assessed by ELISA, from serum of diseased *Vav1;L-gp* mice (n = 6) in comparison to *L-gp* controls (n = 4). Shown are means ± SEM (**** $P < 0.0001$, student's *t* test).
H. RNA-Seq gene expression profiles of Ig heavy chain constant regions obtained from mesenteric nodal tumor material of *Vav1;L-gp* in comparison to $CD19^{+}$ isolated WT splenocytes. CPM: counts

per million, FDR: false discovery rate. Significance was evaluated by student's *t* test with subsequent assessment of the FDR.

I. RNA-Seq gene expression profiles of Ig light chain constant regions obtained from mesenteric nodal tumor material of *Vav1;L-gp* in comparison to $CD19^+$ isolated WT splenocytes. CPM: counts per million, FDR: false discovery rate. Significance was evaluated by student's *t* test with subsequent assessment of the FDR.

Supplemental Figure S8. Transcriptional programs in murine lymphomagenesis

A. Hierarchical clustering of RNA-Seq gene expression profiles obtained from *Vav1;L-gp* (red) and *CD19;L-gp* (blue) mouse models of lymphomagenesis shows clear separation by genotype. Distance measure: 1- Spearman correlation, HC linkage: complete.

B. Heatmap depicting ssGSEA results as normalized enrichment scores (NES) for the indicated pathways and their distribution between lymphomas derived from the *Vav1;L-gp* (green) and *CD19;L-gp* mouse models (orange: PC phenotype, purple: Mature phenotype). All pathways shown are differentially enriched at an FDR < 0.1.

Supplemental Table S1: Primers used in qPCR analysis

Primer name	Primer sequence
L-gp130 fwd (human)	ATG ATA AAG AAT TGT GCG GCG G
L-gp130 rev (human)	TGT TTA AGC TGT GCC ACC TG
gp130 fwd (murine)	CCG TCA TTT TGG ATT TGG CAC A
gp130 rev (murine)	CCT CAC CAG CCC ACA TTC TA
GAPDH fwd (murine)	AAG GTC ATC CCA GAG CTG AA
GAPDH rev (murine)	CTG CCT CAC CAC CTT CTT GA

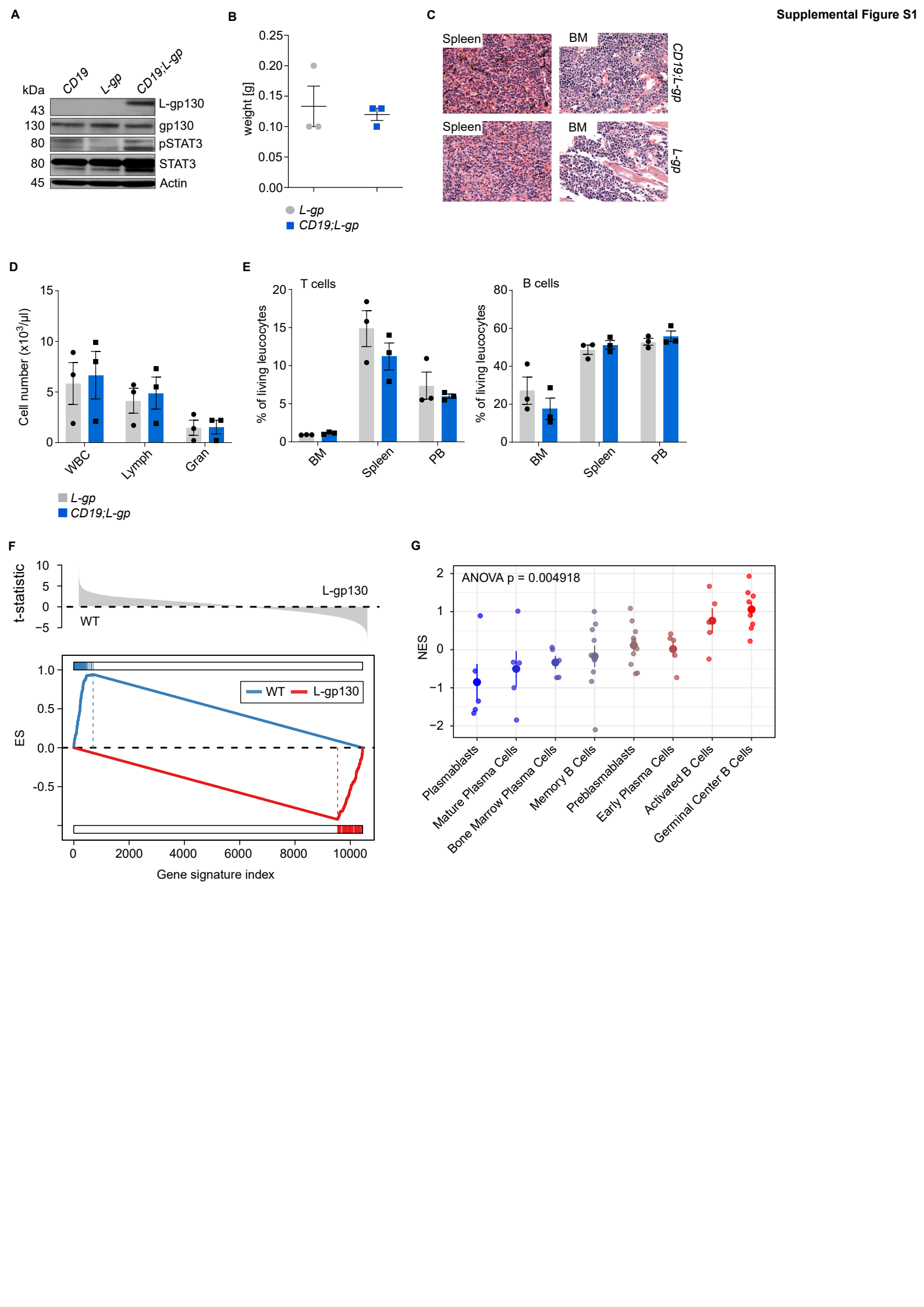
A
kDa
CD19
L-gp
CD19;L-gp
43
130
80
80
45
L-gp130
gp130
pSTAT3
STAT3
Actin
B
weight [g]
0.25
0.20
0.15
0.10
0.05
0.00
L-gp
CD19;L-gp
C
Spleen
BM
CD19;L-gp
Spleen
BM
L-gp
D
Cell number (x10³/µl)
15
10
5
0
WBC
Lymph
Gran
L-gp
CD19;L-gp
E
T cells
% of living leucocytes
20
15
10
5
0
BM
Spleen
PB
B cells
% of living leucocytes
80
60
40
20
0
BM
Spleen
PB
F
t-statistic
10
5
0
−5
L-gp130
WT
ES
1.0
0.5
0.0
-0.5
WT
L-gp130
0
2000
4000
6000
8000
10000
Gene signature index
G
ANOVA p = 0.004918
NES
2
1
0
−1
−2
Plasmablasts
Mature Plasma Cells
Bone Marrow Plasma Cells
Memory B Cells
Preblasmablasts
Early Plasma Cells
Activated B Cells
Germinal Center B Cells

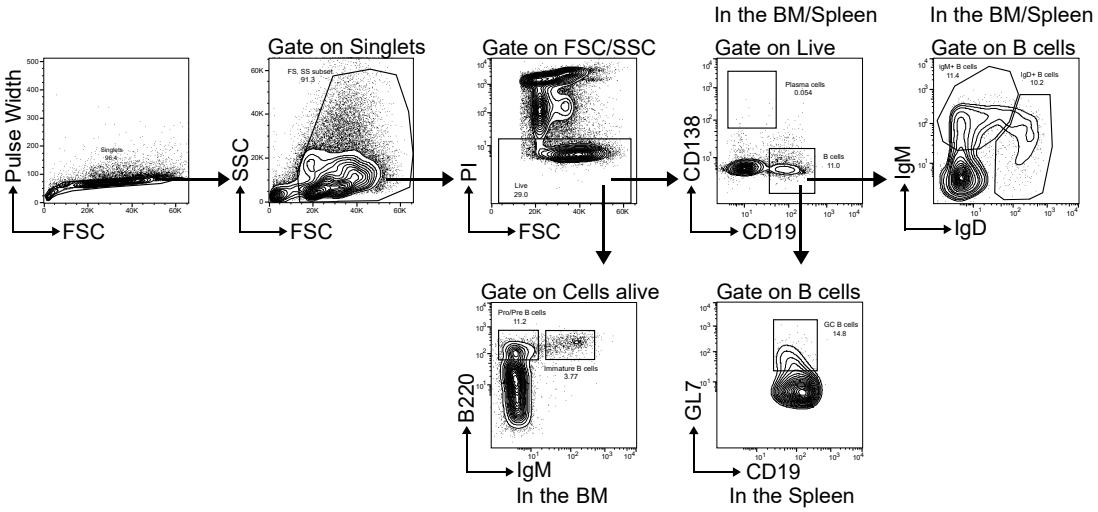
Gate on Singlets
Gate on FSC/SSC
In the BM/Spleen
Gate on Live
In the BM/Spleen
Gate on B cells
Pulse Width
FSC
SSC
FSC
PI
FSC
CD138
CD19
IgM
IgD
Plasma cells
0.054
B cells
11.0
IgM+ B cells
11.4
IgD+ B cells
10.2
Gate on Cells alive
Gate on B cells
B220
IgM
In the BM
GL 7
CD19
In the Spleen
Pro/Pre B cells
11.2
Immature B cells
3.77
GC B cells
14.8

Supplemental Figure S3

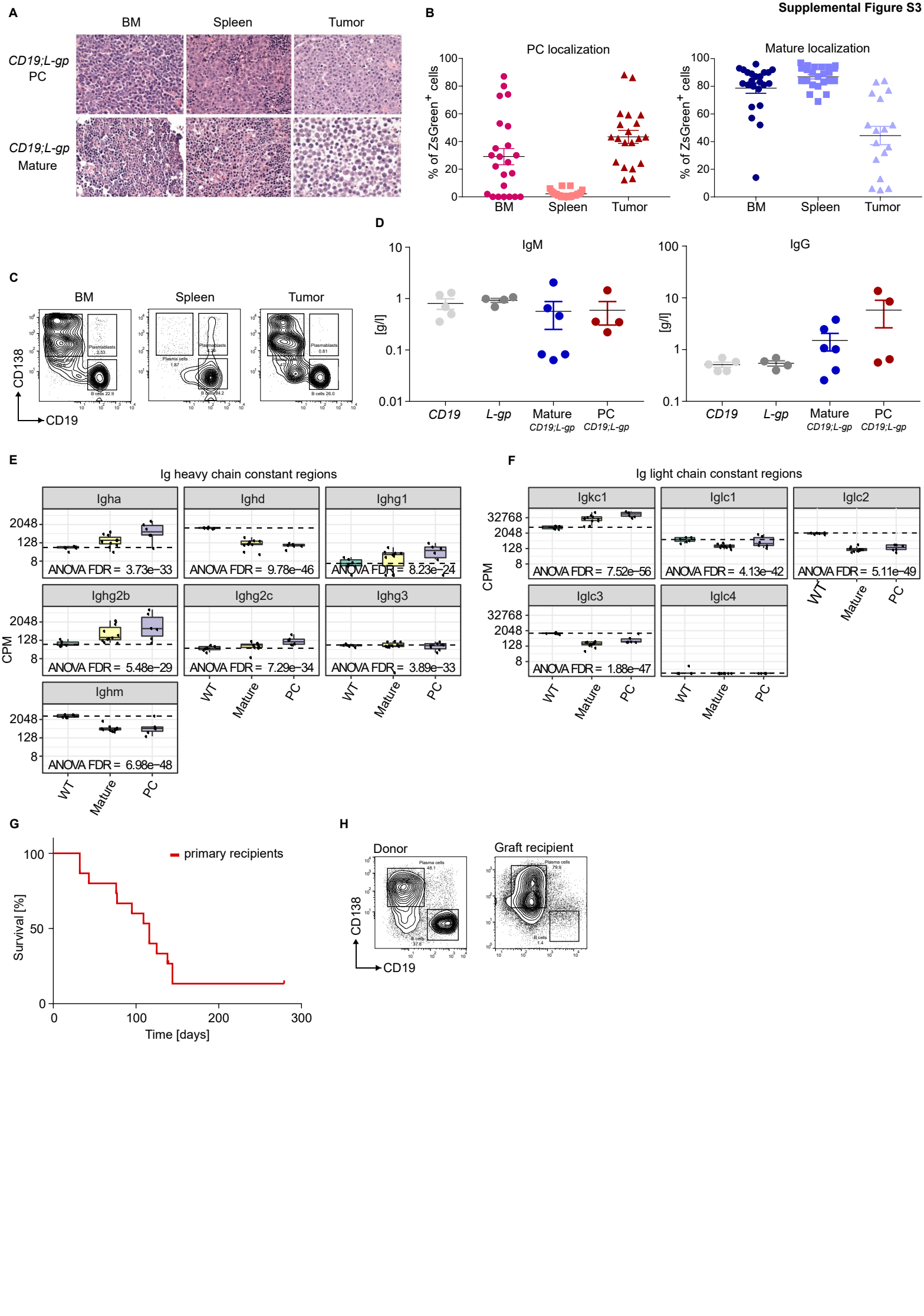

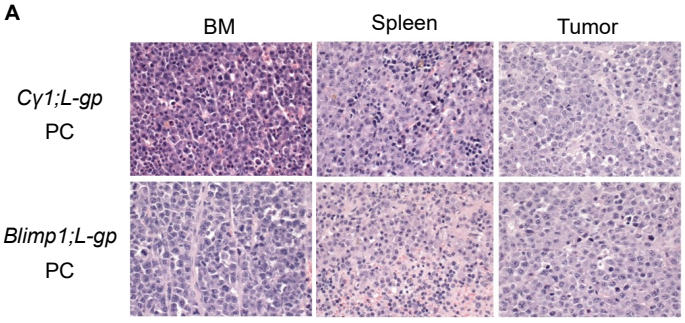
A
BM
Spleen
Tumor
Cγ1;L-gp
PC
Blimp1;L-gp
PC

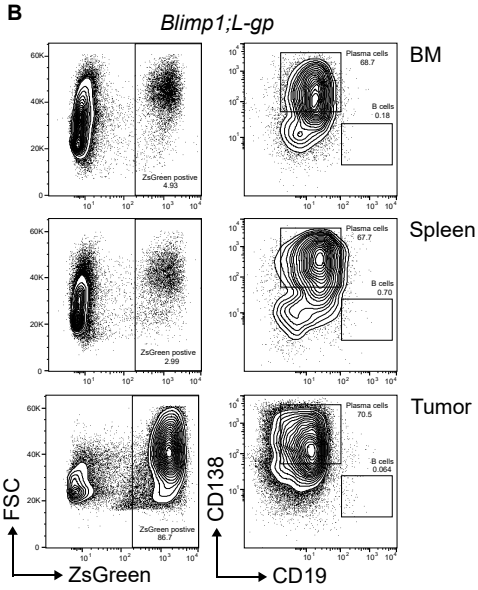
B
Blimp1;L-gp
BM
Spleen
Tumor
FSC
ZsGreen
CD138
CD19

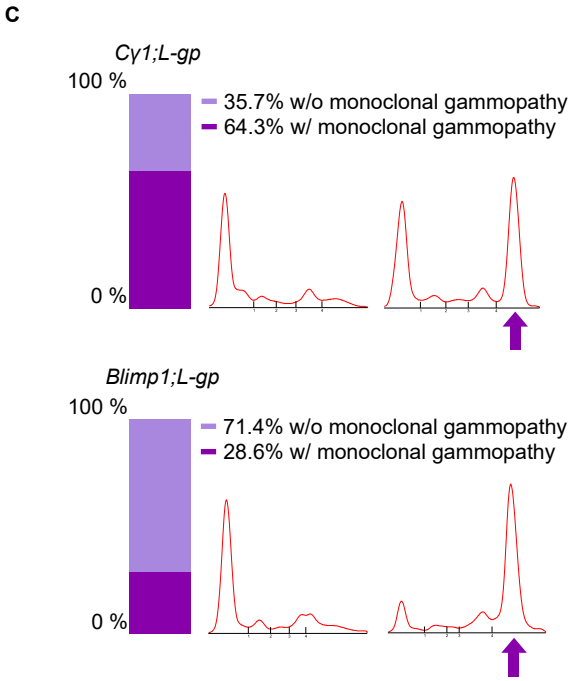
C
Cγ1;L-gp
100 %
0 %
35.7% w/o monoclonal gammopathy
64.3% w/ monoclonal gammopathy
Blimp1;L-gp
100 %
0 %
71.4% w/o monoclonal gammopathy
28.6% w/ monoclonal gammopathy

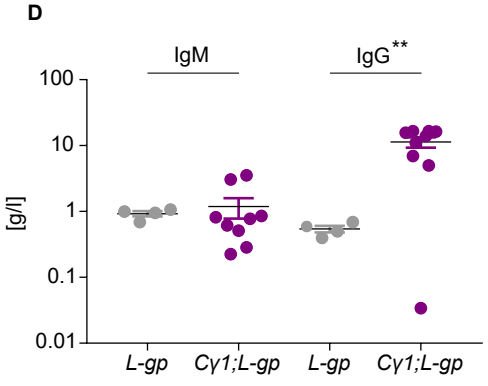
D
IgM
IgG**
100
10
1
0.1
0.01
[g/l]
L-gp
Cγ1;L-gp
L-gp
Cγ1;L-gp

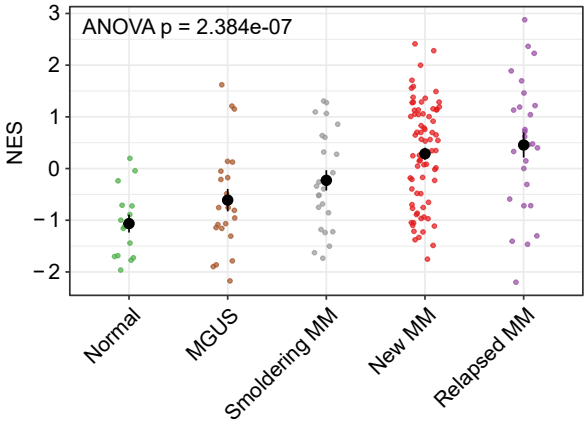
ANOVA p = 2.384e-07
NES
3
2
1
0
−1
−2
Normal
MGUS
Smoldering MM
New MM
Relapsed MM

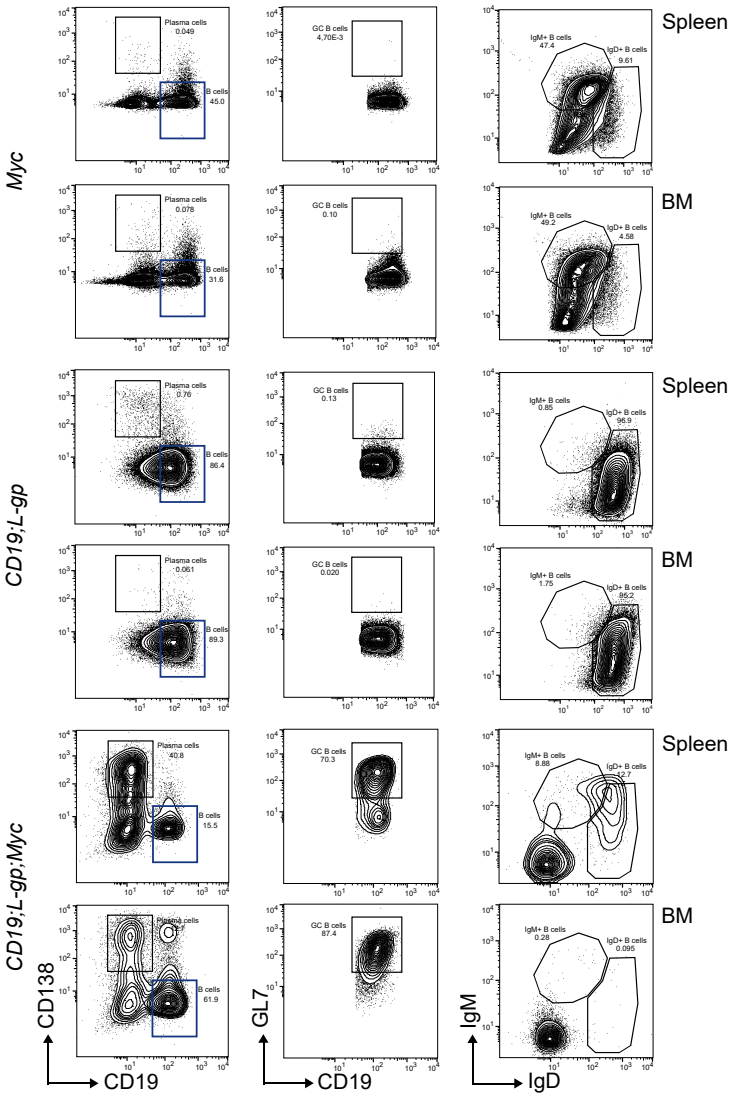
Myc
CD19;L-gp
CD19;L-gp;Myc
Spleen
BM
Plasma cells
0.049
B cells
45.0
GC B cells
4.70E-3
IgM+ B cells
47.4
IgD+ B cells
9.61
Plasma cells
0.078
B cells
31.6
GC B cells
0.10
IgM+ B cells
49.2
IgD+ B cells
4.58
Plasma cells
0.76
B cells
86.4
GC B cells
0.13
IgM+ B cells
0.85
IgD+ B cells
96.9
Plasma cells
0.061
B cells
89.3
GC B cells
0.020
IgM+ B cells
1.75
IgD+ B cells
85.2
Plasma cells
40.8
B cells
15.5
GC B cells
70.3
IgM+ B cells
8.98
IgD+ B cells
52.7
Plasma cells
0.7
B cells
61.9
GC B cells
87.4
IgM+ B cells
0.28
IgD+ B cells
0.095
CD138
CD19
GL7
CD19
IgM
IgD

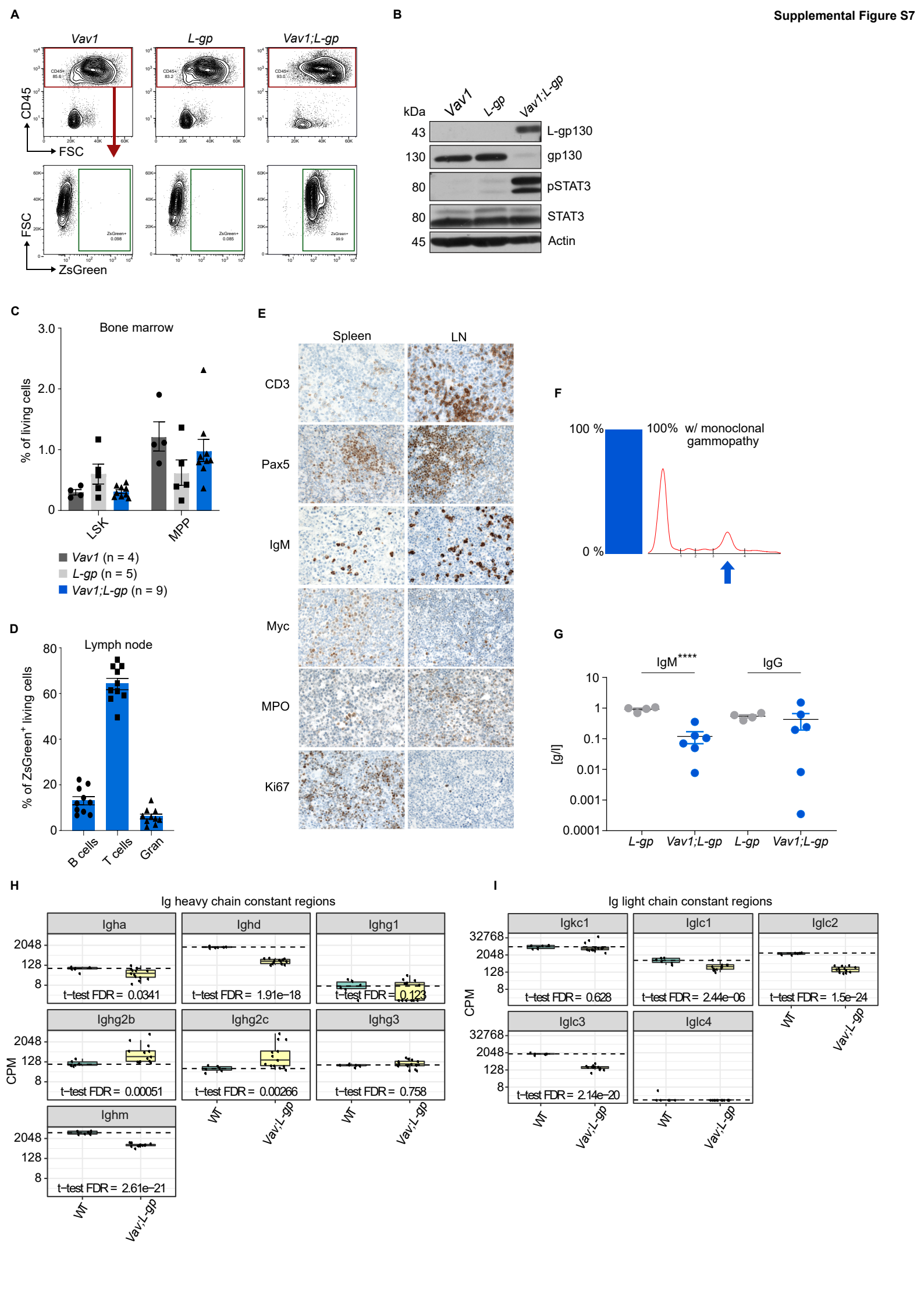
A
Vav1
L-gp
Vav1;L-gp
CD45
FSC
FSC
ZsGreen
B
kDa
Vav1
L-gp
Vav1;L-gp
43
L-gp130
130
gp130
80
pSTAT3
80
STAT3
45
Actin
C
Bone marrow
% of living cells
3.0
2.0
1.0
0
LSK
MPP
Vav1 (n = 4)
L-gp (n = 5)
Vav1;L-gp (n = 9)
D
Lymph node
% of ZsGreen+ living cells
80
60
40
20
0
B cells
T cells
Gran
E
Spleen
LN
CD3
Pax5
IgM
Myc
MPO
Ki67
F
100 %
0 %
100% w/ monoclonal gammopathy
G
IgM****
IgG
[g/l]
10
1
0.1
0.01
0.001
0.0001
L-gp
Vav1;L-gp
L-gp
Vav1;L-gp
H
Ig heavy chain constant regions
Igha
t-test FDR = 0.0341
Ighd
t-test FDR = 1.91e-18
Ighg1
t-test FDR = 0.123
Ighg2b
t-test FDR = 0.00051
Ighg2c
t-test FDR = 0.00266
Ighg3
t-test FDR = 0.758
Ighm
t-test FDR = 2.61e-21
CPM
2048
128
8
WT
Vav;L-gp
I
Ig light chain constant regions
Igkc1
t-test FDR = 0.628
Iglc1
t-test FDR = 2.44e-06
Iglc2
t-test FDR = 1.5e-24
Iglc3
t-test FDR = 2.14e-20
Iglc4
CPM
32768
2048
128
8
WT
Vav;L-gp

Supplemental Figure S8

A

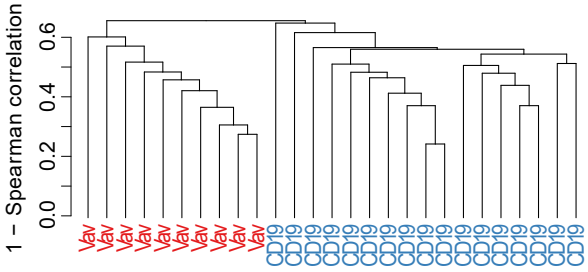

B